Noise Parameters of SIS Mixers

LARRY R. D'ADDARIO

Abstract—**It has been shown that very low noise receivers can be constructed at millimeter wavelengths by using mixers containing superconducting tunnel junctions as the nonlinear elements. This is possible because of both the low intrinsic noise of these devices and their potential for high conversion gain. In this paper the quantum theory of mixing is used to derive the full noise parameters and small-signal parameters of sinusoidally pumped SIS junctions. These are then put into a form that allows the extensive theory of two-port linear networks to be brought to bear, allowing calculation of such useful parameters as minimum noise temperature, optimum source impedance, available (or exchangeable) gain at minimum noise, and stability factor. These quantities are properties of the pumped junction that do not depend on the source or load impedance, but do depend on the terminations at the image and harmonic sideband frequencies. The harmonic sidebands are taken to be shorted, and the image termination dependence is studied in detail. Numerical results are presented for both ideal (BCS theory) and practical (measured current–voltage characteristic) junctions. The noise parameters of the cascade connection of an SIS mixer and a (noisy) IF amplifier are considered, leading to a specification of the optimum coupling network between the two. Finally, it is noted that the SIS mixer is usually not unconditionally stable, but that oscillation can be avoided by careful design of the IF coupling network.**

I. Introduction

IT WAS PREDICTED in 1980 by Tucker [1] that millimeter-wavelength mixers employing superconductor–insulator–superconductor (SIS) junctions would be capable of conversion gain. This was a consequence of the newly developed quantum theory of mixing [2], which applies to two-terminal devices having significant nonlinearity on a voltage scale less than hf_s/q, where f_s is the signal frequency, h is Planck's constant, and q is the electronic charge. Conversion gain was first demonstrated experimentally in 1980 by Shen *et al.* [3], and subsequently the theory has been verified in more detail [4]. Arbitrarily large available gain is possible [1], [5]. The quantum theory also predicts that the noise added in the mixing process will be very small for some junctions. Recently, Feldman [6] has identified circumstances under which this noise achieves the "quantum limit" imposed by the uncertainty principle [7]: any linear amplifier or mixer whose photon number gain is large must add noise with a power spectral density of at least $kT_{ql} = hf_s/2$ to its input, where k is Boltzmann's constant and T_{ql} is defined as the quantum limit noise temperature. Noise temperatures as low as 3.8 K have been measured in laboratory experiments at 36 GHz [8], where $T_{ql} = 1.86$ K. (In this paper, *noise temperature* T will always refer to power spectral density kT, not the power available from a resistor at physical temperature T. This is consistent with the way noise temperature is usually measured, by extrapolating linearly from measurements with two or more high-temperature noise sources to a fictitious source with no noise.) Complete receivers using SIS mixers have been built for radio astronomy at frequencies from 35 to 230 GHz [9]–[15], and several are in regular use on radio telescopes. They are now the lowest noise receivers in this frequency range, although their noise temperatures do not approach the quantum limit.

The noise temperature of a receiver consisting of a mixer cascaded with an IF amplifier is

$$T_{\text{rcvr}} = T_{\text{mxr}} + \frac{T_{\text{amp}}(Y_{\text{out}})}{G_{\text{mxr}}} \tag{1}$$

where T_{mxr} and T_{amp} are the noise temperatures of the mixer and amplifier, respectively, and G_{mxr} is the available gain of the mixer. The amplifier noise depends on its input source admittance, which is the mixer output admittance Y_{out}. T_{mxr}, G_{mxr}, and Y_{out} all depend on the mixer operating conditions; the study of these dependencies for SIS mixers is the main subject of this paper. The lowest possible T_{rcvr} is obtained when $T_{\text{mxr}} = T_{ql}$ and $T_{\text{amp}}/G_{\text{mxr}}$ is negligible. This would seem to be achievable in view of the arbitrarily large gain available from SIS mixers. But, as we shall see, such high gain is always accompanied by low $|Y_{\text{out}}|$, far from the optimum source admittance for which microwave amplifiers are usually designed. This explains the relatively high noise temperatures of some of the receivers so far built; their noise temperatures are dominated by the second term in (1).

For SIS mixers $\text{Re}(Y_{\text{out}})$ can easily be negative. Then (1) remains valid provided that G_{mxr} and T_{amp} are defined in terms of exchangeable power, a generalization of available power due to Haus and Adler [16]. The exchangeable power of a source whose impedance has positive real part is the same as its available power; for negative real part, it is the negative of the maximum power that can be pushed into the source. For a thorough discussion, see [17]. If $\text{Re}(Y_{\text{out}}) < 0$, then both G_{mxr} and T_{amp} are negative.

To the extent that a mixer can be treated as a two-port linear device, the extensive theory of such devices can be used to derive useful quantities. The terminal behavior of a two-port is completely described by a set of four complex signal parameters (such as impedance, admittance, or scattering parameters) and a set of four real noise parameters. Each set has several equivalent forms which are easily

Manuscript received October 4, 1987; revised February 8, 1988.

This work was performed while the author was with the CSIRO Division of Radiophysics, Epping, NSW, Australia; he is presently with the National Radio Astronomy Observatory, Charlottesville, VA 22903.

IEEE Log Number 8821223.

transformed from one to another [18]. A useful set of noise parameters is $\{T_{\min}, T_d, Y_{\text{opt}}\}$ such that

$$T_n = T_{\min} + T_d \frac{|Y_s - Y_{\text{opt}}|^2}{\text{Re}(Y_{\text{opt}})\,\text{Re}(Y_s)} \tag{2}$$

where T_n is the noise temperature of the device and Y_s is the input source admittance. Thus, $T_{\min}$ is the minimum noise temperature, Y_{opt} is the source admittance that achieves this minimum, and T_d is a measure of the noise sensitivity to deviations from Y_{opt}. An important property of these noise parameters is that $T_{\min}$ and T_d are unchanged if the given two-port is cascaded with any noiseless, reciprocal two-port [19]. More generally, given the signal and noise parameters of two two-ports (such as a mixer and IF amplifier), the signal and noise parameters of their cascade combination (or other interconnection) can be computed.

The exchangeable gain and output impedance are also functions of Y_s, determined by the signal parameters. We shall be particularly interested in $G_{\text{mxr}}(Y_{\text{opt}})$, called the associated gain G_a, and in $Y_{\text{out}}(Y_{\text{opt}})$.

There is a general theory about the stability of linear two-ports [20]. Given the signal parameters, a stability factor K can be defined such that if $K > 1$ then the device is *unconditionally stable*; i.e., it will not oscillate with any passive terminations. Often, SIS mixers are only stable for certain terminations (conditionally stable).

II. Calculations

A. Summary of Quantum Mixer Theory

The quantum theory of mixing developed by Tucker [2] follows from expressions first derived by Werthamer [21] for the current in an SIS junction resulting from any given time function of applied voltage. If the voltage consists of a large, periodic waveform of fundamental frequency f_L, plus a small signal at frequency $mf_L + f_0$ for integer m, then the current will consist of components at the frequencies $nf_L + kf_0$ for all integers n, k. In mixer terminology, f_L is the local oscillator (LO) frequency and f_0 is the intermediate frequency (IF) or output frequency. For $m = 1$ the signal is in the upper sideband, for $m = -1$ it is in the lower sideband, and for $|m| > 1$ it is in a higher harmonic sideband. For sufficiently small signal amplitudes the currents at frequencies with $|k| > 1$ can be neglected. All of this applies to a classical (resistive) mixer as well as to a quantum mixer, the difference being that a purely resistive nonlinear device has an instantaneous current that is a (nonlinear) function only of the instantaneous voltage, whereas in an SIS junction the current is given by[1]

$$I(t) = 2\text{Re}\left[\int_{-\infty}^{t} I_{\text{FT}}(t-t')\, e^{i2\pi(q/h)\int_{t'}^{t} V_{\text{ac}}(\tau)\,d\tau}\,dt'\right] \tag{3}$$

[1]This equation is easily derived from Tucker's [2, eqs. (2.8), (2.11), (2.16)] or Werthamer's [21, eqs. (10)–(12)], which appear to be much more complicated because of the introduction of auxiliary functions

where $V_{\text{dc}} + V_{\text{ac}}(t) = V(t)$ is the applied voltage; and $I_{\text{FT}}(t)$ is the Fourier transform of the dc current–voltage characteristic of the junction $I_{\text{dc}}(V)$ with respect to transform variable $f = q(V - V_{\text{dc}})/h$:

$$I_{\text{FT}}(t) = \int_{-\infty}^{\infty} I_{\text{dc}}(V_{\text{dc}} + hf/q)\, e^{-i2\pi ft}\,df.$$

If we now let

$$V(t) = V_{\text{dc}} + V_L \cos 2\pi f_L t + \text{Re}\left(\sum_{m=-\infty}^{\infty} v_m e^{i2\pi f_m t}\right) \tag{4}$$

where $f_m = mf_L + f_0$, then the current can be written

$$I(t) = I_{\text{dc}} + I_L(t) + \text{Re}\left(\sum_{m=-\infty}^{\infty} i_m e^{i2\pi f_m t}\right). \tag{5}$$

Equation (3) can then be used to calculate the LO current $I_L(t)$ and the harmonic sideband current amplitudes i_m. Following standard mixer theory [22], [23], we treat the pumped junction (i.e., the junction with dc bias and LO applied) as a multiport linear network, with each of the harmonic sideband frequencies f_m assigned to a separate port. This artifice is convenient, even though the physical junction has only two terminals. The elements of the admittance matrix of the (fictitious) network, defined by

$$Y_{nm} = i_n / v_m, \qquad \text{with } v_k = 0 \text{ for all } k \neq m, \tag{6}$$

are found after some calculation to be [2, eq. (7.5)]

$$Y_{nm} = \frac{q}{2hf_m} \sum_{p=-\infty}^{\infty} J_p(\alpha) J_{p+n-m}(\alpha) \times \left[\tilde{I}(V_p) - \tilde{I}(V_{p-m} - hf_0/q) - \tilde{I}^*(V_{p+n} + hf_0/q) + \tilde{I}^*(V_{p+n-m})\right] \tag{7}$$

where $J_p(\alpha)$ is the pth order Bessel function of the first kind; $\alpha = qV_L/hf_L$ is the normalized LO voltage; $V_p = V_{\text{dc}} + phf_L/q$; and $\tilde{I}(V)$ is the analytic signal of $I_{\text{dc}}(V)$, given by

$$\tilde{I}(V) = 2\int_0^{\infty} I_{\text{FT}}(t)\, e^{+i2\pi(q/h)(V - V_{\text{dc}})t}\,dt = I_{\text{dc}}(V) + i\text{P}\int_{-\infty}^{\infty} \frac{I_{\text{dc}}(V')}{\pi(V - V')}\,dV'. \tag{8}$$

The latter integral is the Hilbert transform of $I_{\text{dc}}(V)$ (sometimes called the Kramers–Kronig transform).

Strictly, (3) gives the expected value of the current. Fluctuations about this value occur because of the quantization of charge (shot noise) and because of thermal motions. The quantum theory allows these fluctuations to be calculated. They have a continuous frequency spectrum, but only those components near the sideband frequencies are of interest here. In a (small) bandwidth δf near f_m, let the current fluctuation amplitude by δi_m. Then a detailed calculation shows that the correlation matrix of these

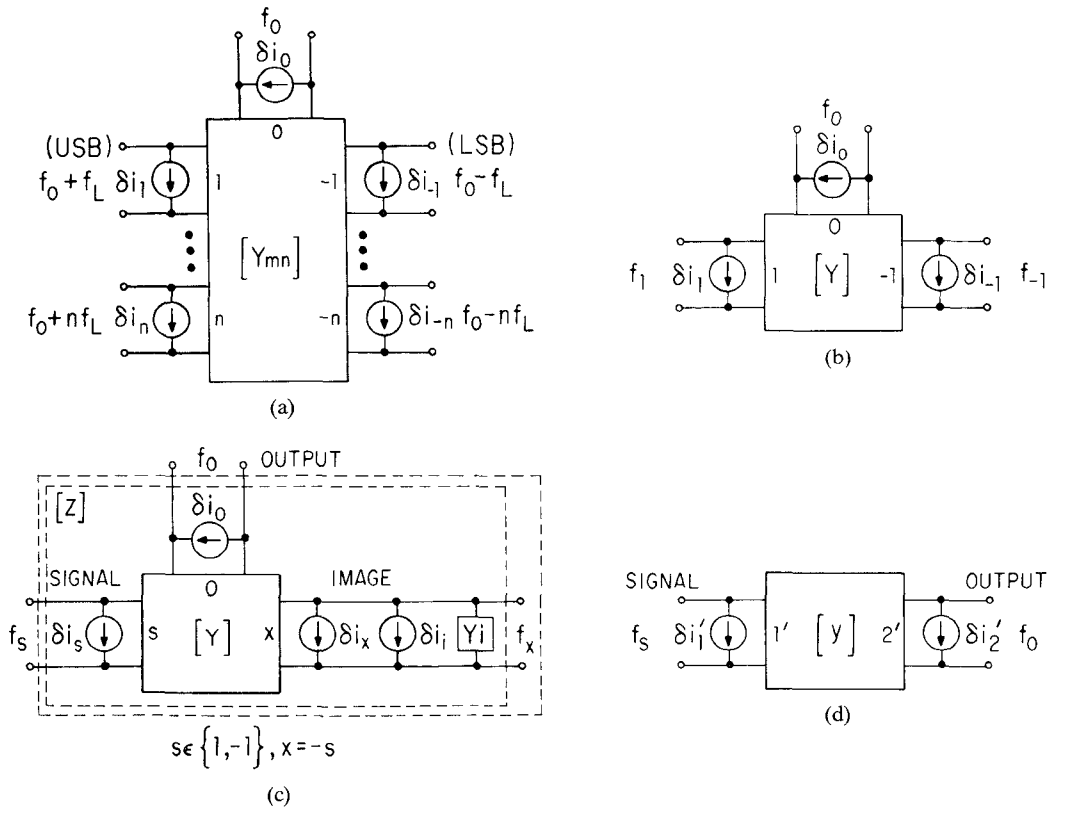

Fig. 1. Development of small-signal and noise model. (a) Multiport network representation including all harmonic sidebands. (b) Three-port model with higher harmonic sidebands shorted. (c) Three-port model with noisy termination on image port. (d) Two-port model equivalent to (c).

current components is [2, eq. (7.16)]

$$H_{nm} = \langle \delta i_n \delta i_m^* \rangle / \delta f$$
$$= q \sum_{p=-\infty}^{\infty} J_p(\alpha) J_{p+n-m}(\alpha)$$
$$\times \left\{ \coth\left[(qV_{p+n} + hf_0)/2kT \right] I_{dc}(V_{p+n} + hf_0/q) \right.$$
$$\left. + \coth\left[(qV_{p-m} + hf_0)/2kT \right] I_{dc}(V_{p-m} + hf_0/q) \right\} \quad (9)$$

where T is the physical temperature of the junction.

Thus, (7)–(9) give a representation of the small-signal and noise behavior of the pumped junction. The model is illustrated in Fig. 1(a).

B. Reduction to Two-Port Model

The network of Fig. 1(a) can be embedded in a larger network, wherein each of the ports is terminated in a finite impedance and one port is connected to the signal source (typically port 1 or -1). The power delivered to the load impedance coupled to the IF port (port 0) due to both the signal and the noise sources can then be calculated. In this way, conversion gain along with very low noise has been predicted for practical junctions by many authors. Here, however, we choose not to jump directly into calculations that depend on the embedding network, but rather to study the properties of the pumped junction itself. Furthermore, unlike most others, we do not assume that f_0 approaches zero.

We first make the justifiable assumption that all ports m with $|m| > 1$ are short-circuited. It happens that this is reasonable for many practical SIS junctions at millimeter wavelengths because the junction construction (typically a parallel-plate sandwich) causes it to be shunted by a substantial, fixed capacitance; the admittance of this capacitor can be mostly canceled at f_L, f_1, and f_{-1}, and is small at f_0, but it forms an effective short at higher frequencies. The current carried by the junction capacitance is not included in $I(t)$ of (3); this simply means that we have, without loss of generality, treated the capacitor as part of the embedding network. Note also that the use of a sinusoidal LO voltage in (2) implies that the LO harmonics nf_L, $n > 1$, are shorted.[2] The signal and noise model of the pumped junction is then reduced to the three-port form of Fig. 1(b), described by the 3×3 matrices $\boldsymbol{Y}$ and $\boldsymbol{H}$, whose components are given by (7) and (9), respectively, for $n, m \in \{-1, 0, 1\}$.

Most of the results of two-port network theory cited earlier are not readily extendable to three-port networks like Fig. 1(b). To make use of these results, select port $s(=1$ or $-1)$ as the signal (input) port, and let port $x = -s$ be the image port. Then connect a fixed admittance Y_t to port x, along with a (noisy) current source

[2] There have been attempts to develop computer codes which relax this assumption [24] and hence treat low-capacitance junctions. It is generally found that poorer mixer performance results, so it is reasonable to restrict our attention to relatively high capacitance junctions

$\delta i_i(t)$ whose mean square value near f_x is $H_i\delta f$, as shown in Fig. 1(c). We will later take this noise source to be the thermal noise of the image termination.

The three-port that includes Y_i has an impedance matrix given by

$$\boldsymbol{Z} = [\boldsymbol{Y}' + \mathrm{diag}(0,0,Y_i)]^{-1} \tag{10}$$

where $\boldsymbol{Y}'$ is the same as $\boldsymbol{Y}$ except that the elements have been reordered so that row and column indices $\{1,2,3\}$ correspond to {signal, image, IF}, respectively. The two-port obtained by leaving port 3 open circuited then has the admittance matrix

$$y = \begin{bmatrix} Z_{11} & Z_{12} \\ Z_{21} & Z_{22} \end{bmatrix}^{-1}. \tag{11}$$

Any two-port linear network can be represented as a noiseless two-port connected to two noise generators in any of several equivalent arrangements [18]. The model of Fig. 1(d), consisting of a two-port with a shunt noise source at each port, is equivalent to the noisy two-port enclosed in the outer dashed box of Fig. 1(c) if the sources are related by

$$\begin{aligned} \delta i_1' &= \delta i_s + (\delta i_x + \delta i_i) R_1 \\ \delta i_2' &= \delta i_0 + (\delta i_x + \delta i_i) R_2 \end{aligned} \tag{12}$$

where

$$R_k = y_{k1}Z_{13} + y_{k2}Z_{23}, \qquad k = 1,2.$$

Then a straightforward calculation shows that the correlation matrix $\boldsymbol{h}$ of these new sources has elements given by

$$\begin{aligned} h_{11} &= H_{11}' + |R_1|^2(H_{33}' + H_i) + 2\mathrm{Re}\{H_{13}'R_1\} \\ h_{22} &= H_{22}' + |R_2|^2(H_{33}' + H_i) + 2\mathrm{Re}\{H_{23}'R_2\} \\ h_{12} &= h_{21}^* = H_{12}' + H_{13}'R_2 + R_1^*H_{32}' + R_1^*R_2(H_{33}' + H_i) \end{aligned} \tag{13}$$

assuming that the image termination noise is uncorrelated with the junction noise. Here the H_{ij}' are the reordered version of H_{nm}, in the same way as $\boldsymbol{Y}'$ relates to Y_{nm}.

If the image termination is at physical temperature T_i, then the full quantum expression for the available thermal noise power in bandwidth δf near f_x is [25]

$$P_a = (hf_x/2)\delta f \coth(hf_x/2kT_i). \tag{14}$$

The mean square spectral density of the equivalent current source is then

$$H_i = 2hf_x\mathrm{Re}(Y_i)\coth(hf_x/2kT_i). \tag{15}$$

Notice that this expression does not vanish at $T_i = 0$; this is because it includes the so-called zero-point fluctuations and is valid at low temperatures and high frequencies. (The familiar classical limit, $P_a = kT_i$, is obtained when $hf_x/kT_i \to 0$.)

The matrices y and $\boldsymbol{h}$ now describe the signal and noise properties of the mixer model shown in Fig. 1(d). They depend only on (a) the dc current–voltage function of the junction, $I_{\mathrm{dc}}(V)$; (b) the frequencies f_L and f_s; (c) the bias voltage V_{dc} and LO amplitude V_L; and (d) the image termination admittance Y_i and its temperature T_i. The practical parameters $T_{\min}$, Y_{opt}, T_d, G_a, and Y_{out} are easily obtained from y and $\boldsymbol{h}$ using standard formulas.

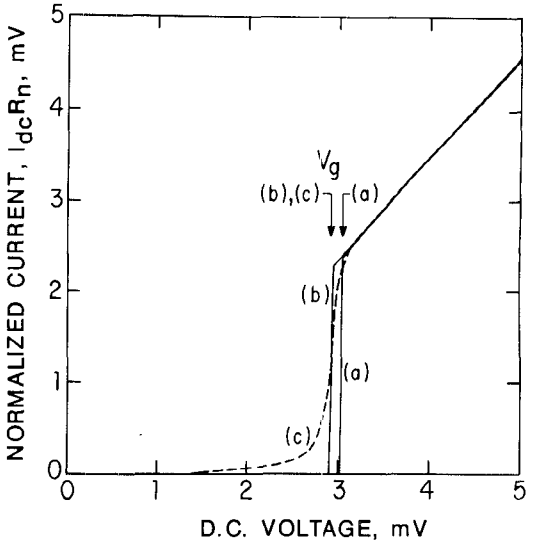

Fig. 2. Current–voltage curves used in the simulations. (a) Calculated curve for BCS superconductors at temperature $T = 0$ and gap voltage $V_g = 3.04$ mV; for $V < V_g$, the current is zero. (b) Calculated at $T = 3.4$ K, $V_g = 2.96$ mV; for $V < V_g$, the current is about 0.02 mV/R_n, which is not visible on this scale. (c) Measured for Pb-alloy junction at $T = 3.4$ K.

III. Numerical Simulations

Numerical calculations of the signal and noise matrices were carried out for three different current–voltage functions (I–V curves), shown in Fig. 2. These included two calculated curves, based on the BCS theory [26], the first for temperature $T = 0$ and the second for $T = 3.4$ K. Each of these was computed from the integral formulas given by Harris [27], assuming identical superconductors with energy gaps $2\Delta = 3.04$ meV at $T = 0$ and 2.96 meV at 3.4 K. The third I–V curve was experimentally measured at $T = 3.4$ K using a lead alloy junction (Pb–In–Au/oxide/Pb–Bi) fabricated by the author at the laboratories of the National Bureau of Standards in Boulder, CO [28]. The energy gap for the theoretical curve at 3.4 K was chosen to match the apparent sum gap of the experimental curve. The value of the 0 K curve was extrapolated according to the BCS dependence for a critical temperature of 7.5 K, near that of the experimental superconductors. In each plot the current is scaled by the normal resistance R_n of the junction, where $1/R_n$ is the asymptotic slope of the curve at high voltages. For our purposes, the significant differences between the three curves are these: the first is "ideal," with zero subgap current and infinite slope at turn on; the second has nonzero subgap current but retains the infinite slope; and the third has still higher subgap current and finite slope.

For each I–V curve, mixer simulations were computed at various LO and intermediate frequencies, and with the signal in each sideband. In most cases, the bias voltage and LO amplitude were held at predetermined values. We used $V_{\mathrm{dc}} = V_g - hf_L/2q$, where V_g is the voltage corresponding

to the sum of the energy gaps (as indicated in Fig. 2). This voltage is in the center of the first "photon step," where the conversion loss and noise are normally low. We used $V_L = 0.1hf_L/q$ for the $T = 0$ theoretical curve, since it has been shown [29], [6] that for such junctions high conversion gain and low noise occur as $V_L \to 0$. For the $T = 3.4$ K curves, both theoretical and measured, we used the results of separate simulations (see below) to select a value of V_L that minimizes $T_{\min}$.

A. Image Termination Admittance

The dependence of various noise parameters on the image termination Y_i is shown in Figs. 3–5. For these calculations we chose $f_L = 200$ GHz so that each junction is well into the quantum regime (hf_L/q large compared to the voltage range over which most of the current rise occurs in $I_{dc}(V)$); and we chose $f_s = 200.1$ GHz so that the signal is in the upper sideband with $f_0 = f_s - f_L$ very small (frequency dependencies will be considered separately). The appropriate physical temperature of each junction was used in (9), and the image termination temperature in (15) was taken to be the same as the junction temperature. In the figures, the functions are plotted on Smith charts (reflection coefficient planes) whose reference impedance is the junction normal resistance R_n; i.e., for independent variable Y the plots are in the plane of $\Gamma = (1 - R_nY)/(1 + R_nY)$.

For the ideal junction at $T = 0$ the simulations show that all four noise parameters are independent of Y_i to within the estimated numerical errors; hence they are not plotted. We find $T_{\min} = 4.18$ K $\approx hf_s/2k = T_{ql}$ (the quantum limit is achieved) and $1/Y_{\text{opt}} = 0.58R_n \approx (2hf_s/q)/I_{dc}(V_{dc} + hf_L/q)$. These agree closely with analytical results given by Feldman [6] for the case $f_0 \to 0$ and $V_L \to 0$. The sensitivity parameter is $T_d = 2.40$ K.

The independence of $T_{\min}$ from Y_i is interesting. When $\text{Re}(Y_i) = 0$, there can be no thermal noise contribution from the image termination, so the junction noise must account for all of $T_{\min} = T_{ql}$. However, when $Y_i \approx Y_{\text{opt}}$ the zero point fluctuations in the termination must contribute about T_{ql} to the noise temperature; thus, at this Y_i the junction noise contribution must be near zero. The junction current is still subject to the fluctuations of (9), but apparently these can be made to cancel at the output frequency. We have verified this in our simulation by artificially setting $H_i = 0$ (no zero point fluctuations in the image termination); we then find $T_{\min} = 0$ at $Y_i = Y_{\text{opt}}^*$.

Fig. 3 shows the $T_{\min}$ dependence for the other two junctions. The theoretical junction achieves its lowest noise when Y_i is near the edge of the Smith chart, where $T_{\min}$ is about 1 K above T_{ql}. The excess is due to shot noise from the (small) dc current that flows at V_{dc} even in the absence of the LO, as well as from the LO induced current. $T_{\min}$ is largest at $Y_i = Y_{\text{opt}}^*$, where the thermal noise from the image termination (at $T_i = 3.4$ K) is largest. Letting $T_i = 0$, $T_{\min}$ becomes essentially independent of Y_i, but remains about 1 K about T_{ql}. Artificially setting $H_i = 0$, we find the lowest $T_{\min} = 0.95$ K at $Y_i = Y_{\text{opt}}^*$. It thus appears that the complete cancellation of junction noise observed for $T = 0$ is not achieved in this case.

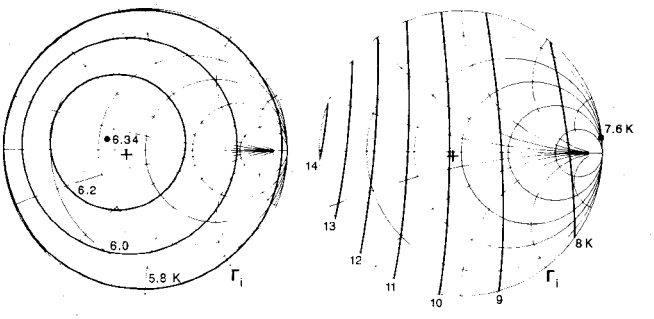

(a) (b)

Fig. 3. Minimum noise temperature versus image termination for junctions and terminations at 3.4 K, $f_L = 200$ GHz, $f_s = 200.1$ GHz, and other parameters as described in the text. The condition $Y_i = Y_s = Y_{\text{opt}}$ is marked with a cross. (a) Theoretical I–V curve from Fig. 2(b). (b) Measured I–V curve from Fig. 2(c). In this and later figures, contours of the dependent variable are plotted on the unit-radius Smith chart of reference impedance R_n. To avoid clutter, the standard constant-impedance circles are not labeled. The independent variable is noted at the lower right corner.

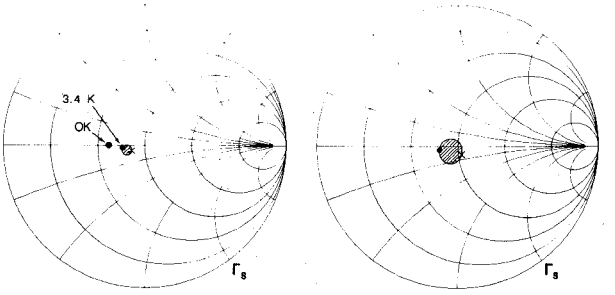

(a) (b)

Fig. 4. Optimum source admittances plotted on the source reflection coefficient plane (note difference from Fig. 3). The hatched region is the range of Y_{opt} for all possible values of Y_i; the points $Y_i = 0$ and $Y_i = \infty$ are marked with a circle and cross, respectively. (a) Theoretical I–V curves. (b) Measured I–V curve.

The measured junction shows noticeably higher noise, largely because of its higher subgap current. The lowest $T_{\min}$, 7.6 K or $1.6T_{ql}$, is produced when Y_i is nearly an open circuit; the lowest T_d (not plotted) is 3.4 K and occurs at the same place. Both parameters increase by less then a factor of two over all Y_i, and reducing the termination temperature from 3.4 K to zero has little effect. Clearly, the junction shot noise dominates.

Fig. 4 shows the range of optimum source admittances Y_{opt} found for each junction. In all cases, Y_{opt} is confined to a small region, although the size of the region increases and shifts toward smaller admittances as the junction quality decreases. In view of the low values of T_d, a source admittance Y_s anywhere in the region would produce a noise temperature very near $T_{\min}$.

For all three junctions the associated gain and output admittance depend strongly on Y_i, as shown in Fig. 5. There is a large region where $\text{Re}(Y_{\text{out}})$ and G_a are negative, bordered by a line where $\text{Re}(Y_{\text{out}})$ passes through zero. Near this line, $|G_a|$ is unbounded. The existence of a negative resistance region in the space of operating param-

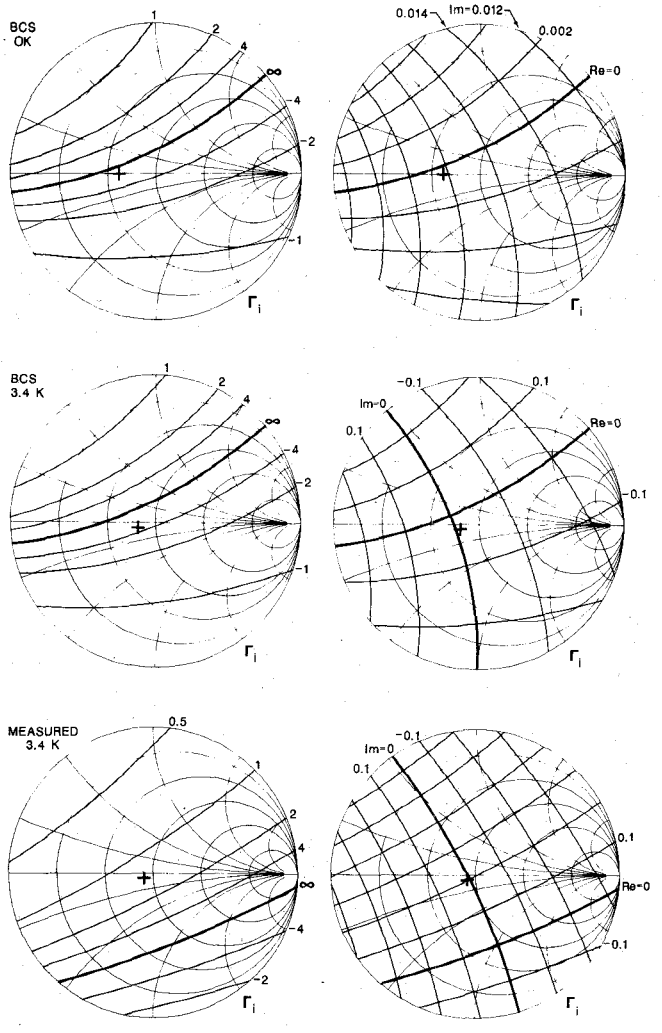

Fig. 5. Associated gain (left) and output admittance (right) versus image termination. Top: theoretical $I-V$ curve at $T=0$. Middle: theoretical at $T=3.4$ K. Bottom: measured $I-V$ curve. The infinite gain contour is plotted as a thick line, and the others are logarithmic. The output admittance is plotted as contours of constant real and imaginary parts, with thick lines for zero; the contour interval is $0.002/R_n$ for the $T=0$ case, and $0.1/R_n$ for the others. A cross indicates where $Y_i = Y_s = Y_{opt}$.

eters of SIS mixers has often been noted. Its significance will be discussed later in connection with stability and IF amplifier noise. Fig. 5 shows that $|G_a|$ is nearly the same for both theoretical junctions, whereas $|Y_{out}|$ is much larger for the $T=3.4$ K one. For the measured $I-V$ curve, the region of negative gain and output conductance is much smaller. The gain appears to depend strongly on the $I-V$ slope at V_g, as might be expected. Neither the gain nor the output admittance appears to be directly affected by the subgap current; it is shown in the next section that the larger output admittance at $T=3.4$ K is due to the larger LO voltage needed to achieve minimum noise.

The output admittance usually has a substantial imaginary part, even though f_0 is very small and even when Y_s and Y_i are real. This can be important when connecting the mixer to an IF amplifier. In the limit $f_0 \to 0$, it can be shown that $\mathrm{Im}(Y_{out}) = 0$ when $Y_i = Y_s^*$, but this limit is not always approached in practice, and it can be advantageous to operate with substantially different Y_i.

The case $Y_i = Y_s = Y_{opt}$ is of particular practical interest because a wide-bandwidth mixer is likely to have equal signal and image terminations. This condition is marked by a cross in Figs. 3 and 5. Y_{opt} is not necessarily the optimum signal admittance under the constraint $Y_i = Y_s$, but for these junctions it appears to be quite close. We find that the theoretical junctions have large, negative gain at this point, whereas the measured junction has small, positive gain.

B. Bias Voltages

The dc bias V_{dc} and LO amplitude (RF bias) V_L affect the noise parameters in a highly nonlinear way. For certain ideal junctions, including our theoretical one at $T=0$, the lowest T_{min} must occur as $V_L \to 0$, since then the LO-induced shot noise is minimized; indeed, we have already shown that the quantum limit is achieved at low V_L. It is also necessary to set the dc bias slightly below V_g, so that there is no dc current in the absence of LO and yet the LO waveform samples the upper portion of the curve during part of the cycle. Under these constraints, we obtain $T_{min} = T_{ql}$ for a wide range of V_{dc} and V_L. Furthermore, perhaps surprisingly, the associated gain remains high even as $V_L \to 0$.

For even slightly nonideal junctions, such as our theoretical one at $T=3.4$ K, the situation is more complicated. The lowest T_{min} occurs at nonzero V_L, and is more sensitive to the choice of V_{dc}. This can be seen in Fig. 6, where T_{min} and G_a are plotted as functions of V_{dc} and V_L with $Y_i = 0$ (open-circuited image) for both the theoretical and measured junctions. The lowest T_{min} is obtained when $\alpha = qV_L/hf_L$ is near 0.7 for the theoretical junction and near 1.4 for the measured junction; these values change very little at other image admittances, so they are the values used in the other simulation studies of this paper. It can be seen that our choice of V_{dc} at the center of the first photon step does not quite minimize T_{min}, but it remains close to the minimum for all image terminations.

A rough understanding of this behavior may be had from the following argument. The component of the junction's current fluctuations due to I_{dc} has a flat power spectrum, and so it is just as significant at f_0, the IF, as at the signal and image frequencies. Since noise temperature is referred to the input, this IF noise can be overcome if there is sufficient gain. (Of course, gain is also needed to overcome the noise of the following amplifier, but at this point we are concerned only with the mixer noise.) Thus, the lowest noise should be obtained for regions of (V_{dc}, V_L)-space where gain G_a is high. However, since I_{dc} is partly due to rectified LO power, the lowest possible V_L should be used. For the theoretical junction, which has a discontinuity in current at V_g, the gain remains fairly constant as $V_L \to 0$, and the noise decreases as expected until about $\alpha = 0.7$; below this point the noise increases, and at present this is not understood. The measured junction, which has a finite slope in its $I-V$ curve at all voltages, shows maximum gain and minimum noise at

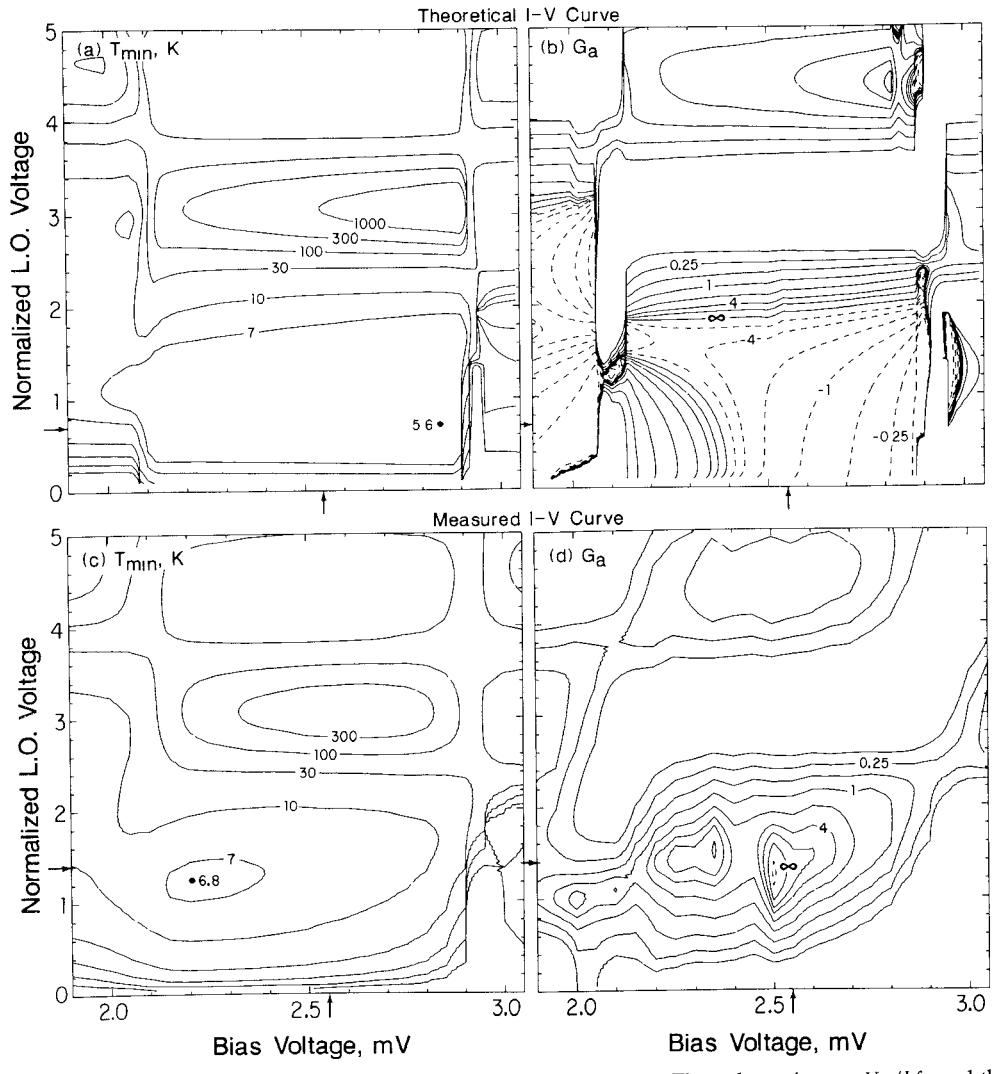

Fig. 6. Contours of constant $T_{\min}$ and G_a versus V_{dc} and V_L for two junctions. The ordinate is $\alpha = qV_L/hf_L$ and the absicca is V_{dc} in mV; values used in the other simulations are marked by arrows. Negative gain contours are dashed lines. All plots were calculated for $f_L = 200$ GHz, $f_s = 200.1$ GHz, $Y_t = 0$. (a), (b): Theoretical $I-V$ at $T = 3.4$ K. (c), (d): Measured $I-V$.

nearly the same V_L. In this case, higher LO voltage is needed to pump the weaker nonlinearity.

In order to compare the two theoretical junctions more closely we also simulated the $T = 0$ junction with $\alpha = 0.7$. It is found that Y_{opt}, Y_{out}, and G_a become essentially identical for the two junctions; thus, the signal parameters are not significantly affected by the small subgap current. The noise temperatures $T_{\min}$ and T_a are increased by 0.5 K and 0.1 K, respectively; the minimum noise of the 3.4 K junction remains about 0.5 K higher (Fig. 3(a)), and only this small excess can be attributed to the intrinsic junction noise.

C. Stability

We have seen that the output admittance of an SIS mixer sometimes has negative real part when the source admittance has been chosen for minimum noise. The IF load impedance must then be carefully chosen if oscillations are to be avoided. It might seem that a good alternative would be to avoid this unstable region by selecting V_{dc}, V_L, and Y_t so that $\mathrm{Re}(Y_{out}) > 0$ at $Y_s = Y_{opt}$, especially since the condition can often be achieved with $T_{\min}$ near its lowest value. But in practice this is not sufficient to ensure stability, because: firstly, the biases and admittances may need to be adjusted before the desired values are achieved, and if the circuit becomes unstable during this process then the correct values may never be found; and secondly, even if conditions are established that ensure stable operation at one input frequency, the circuit may be unstable at other frequencies where the embedding admittances are quite different, including frequencies well outside the band of interest. It is therefore important to inquire whether an SIS junction can be unconditionally stable within a useful and practical range of V_{dc}, V_L, and Y_t.

The stability of a two-port may be fully characterized by Rollett's invariant stability factor [20], defined by

$$K = \frac{2\,\mathrm{Re}(y_{11})\,\mathrm{Re}(y_{22}) - \mathrm{Re}(y_{12}y_{21})}{|y_{12}y_{21}|}. \qquad (16)$$

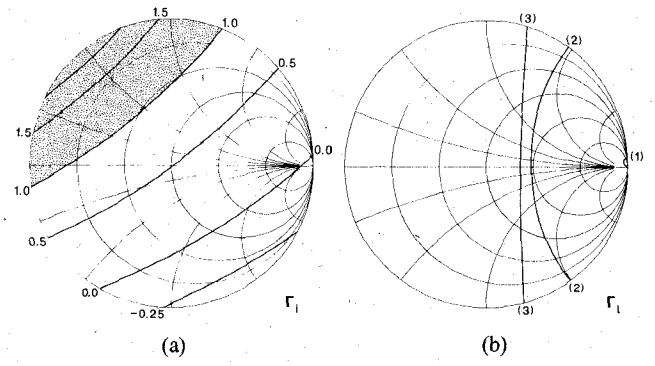

Fig. 7. (a) Stability factor K versus image termination reflection coefficient for measured junction. The region of unconditional stability is shaded. For the theoretical junctions, no stable region was found. (b) $K=1$ contours versus IF load reflection coefficient for each of the junctions. The stable region is to the left of each contour. (1) Theoretical junction, $T=0$ (unstable region very small); (2) theoretical junction, $T=3.4$ K; (3) measured junction.

The two-port is unconditionally stable provided that $\mathrm{Re}(y_{11})>0$, $\mathrm{Re}(y_{22})>0$, and $K>1$.

Stability factor K was computed for the simulations of Figs. 3–5, i.e., for each of the three junctions at $f_L=200$ GHz with fixed biases in the low-noise region. It is found that there is *no* value of Y_i that gives unconditional stability for either of the theoretical junctions under these conditions, and that the stable region for the measured junction is fairly small (Fig. 7a). Larger stable regions could probably be found if V_{dc} and V_L were varied, or if the $I-V$ curves were less sharp compared with hf_L/q, but all of these lead to higher noise.

Since it is not possible to guarantee stability for all source and load admittances, what admittances can be used? We could consider limiting the range of Y_s, Y_i, and/or Y_l, where Y_l is the IF load admittance. It is most practical to limit Y_l, because in most cases $f_0 \ll f_L$, so that Y_l can be set more accurately by the designer than either Y_s or Y_i. This is especially true when $f_L>100$ GHz, where fabrication tolerances are often a significant fraction of a wavelength. We therefore assume that Y_s and Y_i may differ substantially from the desired values or that they may require adjustment over a wide range, whereas we assume that Y_l can be specified in advance. Under these circumstances it is useful to consider a new two-port formed from the three-port mixer model of Fig. 1(b) by connecting a fixed termination to the IF port rather than to the image port. If this two-port is unconditionally stable, then the mixer is stable for any Y_s and Y_i. The stability factor for this new two-port is shown for each of the junctions in Fig. 7(b).

It appears from Fig. 7(b) that the $T=0$ theoretical junction is more stable than the others, in that its region of unconditional stability covers most of the Y_l Smith chart. But this comes from the use of R_n as the reference impedance for the charts; Fig. 5 shows that the output admittance Y_{out} remains well below $1/R_n$ for the $T=0$ junction, but is 50 to 100 times larger for the other junctions.

D. Frequency and Sideband

Simulations were carried out for the same three $I-V$ curves at LO frequencies of 50 and 100 GHz as well as 200 GHz, for IF's up to 20 GHz, and for lower sideband as well as upper sideband signals. The results are qualitatively similar to those already presented, except for the following points.

With lower sideband signals at small f_0 the sign of the reactive part of all admittances is reversed. For example, it can be seen from Fig. 4 that the optimum admittance tends to be slightly capacitive for the upper sideband case; for lower sideband signals it is slightly inductive. Similarly, the output admittance for a given signal and image admittance is conjugated.

T_{min} is nearly proportional to f_s, as is T_{ql}, and hence T_{min} is slightly lower in the lower sideband. This holds for all three junctions simulated here. However, for the measured $I-V$ curve only, T_{min} departs further from T_{ql} as f_L is decreased, and the region of high gain is reduced; at 50 GHz, the lowest T_{min} is about 8 K and no region of negative G_a was found. This junction is then near the limit of quantum mixing effects, and it is behaving more and more like a classical resistive mixer as hf_L/q becomes small compared to the region of rapid current rise on the $I-V$ curve.

IV. Coupling to an IF Amplifier

The usual reason for using a mixer as part of a sensitive receiver is to convert the signal to a frequency where it can be more easily analyzed. The mixer output must therefore be connected to some (necessarily noisy) signal processing circuitry, typically beginning with a low noise amplifier. Whatever the nature of this processing, we shall call it the "IF amplifier" and assume only that it can be treated as a noisy two-port linear network.

The noise temperature of the cascade combination is given by (1). We have seen that it is possible to have $T_{\mathrm{mxr}} \sim T_{ql}=4.8$ K at 200 GHz. Practical microwave amplifiers can have $T_{\mathrm{amp}}<10$ K at frequencies $f_0<10$ GHz if they are cryogenically cooled [30]; in fact, $T_{\mathrm{amp}} \approx 3.5$ K has been achieved at 1.5 GHz [31]. Nevertheless, the second term of (1) will dominate if $G_{\mathrm{mxr}} \ll 1$, so that achieving high mixer gain is at least as important to the overall receiver noise as is achieving low mixer noise. It should be emphasized that it is the *exchangeable gain* [17] (exchangeable output power power divided by power available from input source) that matters here, not the transducer gain (power delivered to output load divided by power available from input source); in many earlier papers on SIS mixers only transducer gain was considered. In addition, T_{amp} may be much larger than its minimum value if Y_{out} is far from the amplifier's optimum source admittance. Since T_{mxr}, G_{mxr}, and Y_{out} all depend on the mixer's operating parameters, it is not at all obvious from (1) what mixer parameters will lead to the lowest T_{rcvr}.

Let the noise parameters of the amplifier be $\{T^a_{\mathrm{min}}, T^a_d, Y^a_{\mathrm{opt}}\}$, and let those of the complete receiver be

$\{T^r_{\min}, T^r_d, Y^r_{\text{opt}}\}$. Then, using (2) for both the mixer and amplifier, we have

$$T_{\text{rcvr}} = T_{\min} + T_d \frac{|Y_s - Y_{\text{opt}}|^2}{\text{Re}(Y_s)\,\text{Re}(Y_{\text{opt}})} + \frac{T^a_{\min}}{G_{\text{mxr}}} + \frac{T^a_d |Y_{\text{out}} - Y^a_{\text{opt}}|^2}{G_{\text{mxr}}\,\text{Re}(Y_{\text{out}})\,\text{Re}(Y^a_{\text{opt}})} \tag{17}$$

$$= T^r_{\min} + T^r_d \frac{|Y_s - Y^r_{\text{opt}}|^2}{\text{Re}(Y_s)\,\text{Re}(Y^r_{\text{opt}})}. \tag{18}$$

Now consider the introduction of a lossless coupling network between the mixer and amplifier. If we regard the coupling network as part of the amplifier, then $T^a_{\min}$ and T^a_d are unchanged, and Y^a_{opt} can be transformed to any desired value by proper choice of the network. Thus the coupling affects only the last term in (17). This term has two extrema as a function of Y^a_{opt}, at $Y^a_{\text{opt}} = Y_{\text{out}}$ and at $Y^a_{\text{opt}} = -Y^*_{\text{out}}$. If $\text{Re}(Y_{\text{out}}) > 0$, then the first case yields minimum amplifier noise $T_{\text{amp}} = T^a_{\min}$; but if $\text{Re}(Y_{\text{out}}) < 0$, the second case yields minimum absolute value of amplifier noise with

$$T_{\text{amp}} = T^a_{\text{neg}} = T^a_{\min} - 4T^a_d < 0. \tag{19}$$

If the coupling network is selected in this optimum way, (17) reduces to

$$T_{\text{rcvr}} = T_{\min} + T_d \frac{|Y_s - Y_{\text{opt}}|^2}{\text{Re}(Y_s)\,\text{Re}(Y_{\text{opt}})} + \frac{1}{G_{\text{mxr}}} \times \begin{cases} T^a_{\min}, & \text{if } G_{\text{mxr}} > 0 \\ T^a_{\text{neg}}, & \text{otherwise} \end{cases} \tag{20}$$

where we have used the fact that G_{mxr} and $\text{Re}(Y_{\text{out}})$ have the same sign. For a given amplifier either $T^a_{\min}$ or $|T^a_{\text{neg}}|$ might be smaller ([32] gives an example of each case).

However, there are other constraints on the design of the coupling network. If the stability criterion adopted in Section III-C is to be satisfied, then the load admittance Y_l must be kept large. But since Y_{out} is small in the region of high $|G_{\text{mxr}}|$, we desire Y^a_{opt} to be small. The usual practice in designing low-noise amplifiers is to attempt to make the input admittance equal to the optimum admittance (and both equal to a convenient transmission line characteristic admittance), and yet we have found that just the opposite is required here. If $Y^a_{\text{opt}} = Y_l$ for the original amplifier, then the coupling network can transform both to another admittance, but they will still be equal. However, the amplifier need not have this property. The active devices used in microwave amplifiers (especially FET's and HEMT's) often have quite different intrinsic input and optimum admittances; furthermore, a more general lossless embedding network than our coupling network (including feedback) can allow Y^a_{opt} and Y_l to be set separately, within practical limits. This suggests that a practical design approach would be the following. For fixed active devices in the amplifier, embed them in a network which achieves an input admittance Y_l that is safely inside the region of unconditional stability for the mixer; under this constraint, adjust the optimum source conductance $\text{Re}(Y^a_{\text{opt}})$ to be as small as possible. If the embedding network is lossless, then the noise parameters $T^a_{\min}$ and T^a_d will be determined only by the active devices.

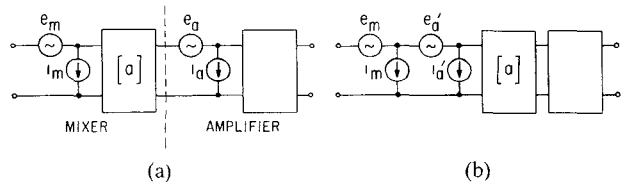

Fig. 8 Noise model for mixer-amplifier cascade (a) Noise sources at input of each device. (b) All noise sources transformed to mixer input.

Having selected the best practical IF amplifier and coupling network, we can minimize the receiver noise by adjusting the mixer parameters V_{dc}, V_L, Y_t, and Y_s. This will result in a tradeoff between the mixer's contribution (first two terms of (17)) and the amplifier's contribution. To investigate this further, we shall need the noise parameters of the complete receiver. Consider the model of Fig. 8(a) where the noises of the mixer and amplifier are represented by current and voltage sources at each of their respective inputs. (The mixer noise sources e_m and i_m can easily be related to the sources $\delta i'_1$ and $\delta i'_2$ in Fig. 1(d).) The correlation matrix of the amplifier noise sources is [33]

$$\boldsymbol{n}_a = \begin{bmatrix} \langle e_a^2 \rangle & \langle e_a^* i_a \rangle \\ \langle e_a i_a^* \rangle & \langle i_a^2 \rangle \end{bmatrix} = k \begin{bmatrix} 4T^a_d/G^a_{\text{opt}} & T^a_{\min} - 4T^a_d Y^a_{\text{opt}}/G^a_{\text{opt}} \\ T^a_{\min} - 4T^a_d Y^a_{\text{opt}}{}^*/G^a_{\text{opt}} & 4T^a_d |Y^a_{\text{opt}}|^2/G^a_{\text{opt}} \end{bmatrix} \tag{21}$$

where $Y^a_{\text{opt}} = G^a_{\text{opt}} + iB^a_{\text{opt}}$. Similarly, let $\boldsymbol{n}_m$ be the corresponding matrix for the mixer.

The amplifier noise sources can be replaced by equivalent sources at the mixer input, as shown in Fig. 8(b), where

$$\begin{bmatrix} e'_a \\ i'_a \end{bmatrix} = \boldsymbol{a} \begin{bmatrix} e_a \\ i_a \end{bmatrix}, \text{ with } \boldsymbol{a} = -\frac{1}{y_{21}} \begin{bmatrix} y_{22} & 1 \\ y_{11}y_{22} - y_{12}y_{21} & y_{11} \end{bmatrix}. \tag{22}$$

$\boldsymbol{a}$ is called the cascading matrix of the mixer. These noise sources have correlation matrix [33]

$$\boldsymbol{n}'_a = \boldsymbol{a}\boldsymbol{n}_a\boldsymbol{a}^T \tag{23}$$

where superscript T denotes the conjugate transpose. The sources of Fig. 8(b) can be replaced by a single pair $e_r = e_m + e'_a$, $i_r = i_m + i'_a$, representing the noise of the complete receiver. Since the mixer and amplifier noise sources are independent, the correlation matrices simply add, giving

$$\boldsymbol{n}_r = \boldsymbol{n}_m + \boldsymbol{a}\boldsymbol{n}_a\boldsymbol{a}^T. \tag{24}$$

This is the generalization of the simple noise cascading formula (1). From $\boldsymbol{n}_r$, we can find the practical noise parameters of the receiver $\{T^r_{\min}, T^r_d, Y^r_{\text{opt}}\}$.

TABLE I
RECEIVER NOISE SIMULATIONS

	T_{min} K	T_d K	Y_{opt} mS	G_{mxr}	T_{amp} K
SIS junction only, 208.5 GHz	7.96	3.60	$24.2+i0.72$	+6.11	
HEMT only, 8.5 GHz	10.3	3.45	$1.48-i5.48$		
Cascade directly	150	39.1	$20.4-i0.11$	+21.4	3026
Cascade with shunt L	21.3	7.49	$17.1+i0.18$	+266	3439
Cascade with optimum Y_t	19.5	6.98	$17.5-i2.00$	−1.86	−19.6

The SIS junction parameters are computed from the measured $I-V$ curve with $f_L = 200$ GHz, $f_0 = 8.5$ GHz, $V_{dc} = 2.535$ mV, $\alpha = 1.4$, $R_n = 68.8\Omega$. For all but the last line, $Y_t = 0$. The HEMT is a Fujitsu FHR01FH with noise parameters at 8.5 GHz from [30]. The "shunt L" is a parallel inductor of 0.34 nH, and the "optimum Y_t" is $Y_t = +i5.96$ mS

Simulations of the receiver noise parameters have been calculated in this way for a few interesting cases. An example is given in Table I, where the measured noise parameters of a cryogenically cooled HEMT [30] at 8.5 GHz are used along with calculated noise parameters for the measured SIS $I-V$ curve of this paper at $f_L = 200$ GHz. It can be seen that if the HEMT is connected directly to the SIS junction (no coupling network) then there is a very large noise contribution from the amplifier because Y_{out} is far from Y^a_{opt}. If a shunt inductor is connected at the HEMT input so that Y^a_{opt} becomes nearly real, then the receiver noise is much reduced, although the amplifier noise actually increases. In this case lower overall noise is obtained by setting the source admittance for high mixer gain and accepting high amplifier noise. If the mixer parameters are then varied Y_{out} can be brought closer to Y^a_{opt}, but at a sacrifice in T_{mxr} and G_{mxr}. The last line of Table I shows the result of optimizing T^r_{min} by varying only the image termination; here the tradeoff favors low $|G_{mxr}|$ and low $|T_{amp}|$.

V. PRACTICAL CONSIDERATIONS

A. Image Termination

This paper has shown that the performance of an SIS mixer depends strongly on the image admittance Y_i. But in practice it is difficult to construct a millimeter-wavelength circuit (whether in waveguide or in planar transmission lines or in some combination thereof) in which the admittances at two nearby frequencies like f_s and f_i are separately determined. Typically, one obtains either a broad-band circuit in which the admittances are nearly equal, or a narrow-band circuit in which the admittance at one frequency is tuned to the desired value but the admittance at the other frequency is uncontrolled. Since SIS junctions usually include a large shunt capacitor, narrow-band circuits often result in the junction's being nearly shorted at the uncontrolled frequency. As Figs. 3 and 5 show, a shorted image port is nearly the poorest choice with respect to noise and gain for practical junctions, although it results in better stability (Fig. 7(a)). If a broad-band circuit with $Y_i = Y_s = Y_{opt}$ can be realized, it would seem to be better; but it is then necessary to keep the image termination cold in order to minimize its thermal noise. Since signal and image (and perhaps LO) usually share a single physical port (e.g., waveguide), a low-loss, cold filter is required.

B. Bandwidth and Out-of-Band Frequencies

The calculations of this paper have been done for a single input frequency or output frequency, but in reality a band of frequencies in involved. The optimum source admittance of a pumped SIS junction varies little over a wide range of f_0, but the input circuit can approximate it only over a finite bandwidth. Similarly, the IF amplifier, including its coupling network, will produce low noise and sufficient gain only over a finite bandwidth. Either the input circuit or the IF amplifier might limit the useful bandwidth of the receiver. There is usually a band of interest for the application, and the designer attempts to make the useful bandwidth cover this band. But even if he succeeds in this, problems may arise at frequencies outside the band of interest. This is particularly true of stability; designers of high-gain microwave amplifiers are well aware of the problem of out-of-band oscillations, and the same problem occurs in SIS mixers that have the potential of high gain over a wide bandwidth. The mixer can still be stabilized by maintaining sufficiently large load admittance Y_l (Fig. 7(b)), but it is important to realize that this must be done over the full range of f_0 where there is potential instability, not just over the band of interest.

Another out-of-band problem with SIS mixers is saturation. Although not otherwise discussed in this paper, it is worth pointing out that if the input to an SIS mixer consists of broad-band noise at high equivalent temperature, then sufficiently high rms signal voltage may develop across the junction so that it can no longer be treated as a linear device. In practical circuits, the highest voltages usually occur at the IF. This can be minimized by keeping Y_l large, but again this must be done for all significant frequencies, since saturation at out-of-band frequencies will also affect the performance in the band of interest [34].

ACKNOWLEDGMENT

The author would like to thank the CSIRO Division of Radiophysics for the opportunity to pursue these studies during a visiting appointment, and for the use of ap-

propriate computing facilities; J. Archer and R. Batchelor for valuable discussions; and the National Bureau of Standards at Boulder, CO, for the use of their fabrication facilities to produce integrated circuits containing SIS junctions.

REFERENCES

[1] J. R. Tucker, "Predicted conversion gain in S–I–S quasiparticle mixers," *Appl. Phys. Lett.*, vol. 36, pp. 477–479, 1980.
[2] J. R. Tucker, "Quantum limited detection in tunnel junction mixers," *IEEE J. Quantum Electron.*, vol. 6, pp. 1234–1258, 1979.
[3] T.-M. Shen, P. L. Richards, R. E. Harris, and F. L. Lloyd, "Conversion gain in mm-wave quasiparticle heterodyne mixers," *Appl. Phys. Lett.*, vol. 36, pp. 777–779, 1980.
[4] S. Rudner, M. J. Feldman, E. Kollberg, and T. Cleason, "The antenna-coupled SIS quasiparticle array mixer," *IEEE Trans. Magn.*, vol. MAG-17, pp. 690–693, 1981; also *J. Appl. Phys.*, vol. 52, p. 6366, 1981.
[5] A. R. Kerr, S.-K. Pan, M. J. Feldman, and A. Davidson, "Infinite available gain in a 115 GHz SIS mixer," *Physica*, vol. 108B, pp. 1369–1370, 1981.
[6] M. J. Feldman, "Quantum noise in the quantum theory of mixing," *IEEE Trans. Magn.*, vol. MAG-23, pp. 1054–1057, 1987.
[7] C. M. Caves, "Quantum limits on noise in linear amplifiers," *Phys. Rev. D*, vol. 26, pp. 1817–1839, 1982.
[8] D. W. Face, D. E. Prober, W. R. McGrath, and P. L. Richards, "High quality tantalum superconducting tunnel junctions for microwave mixing in the quantum limit," *Appl. Phys. Lett.*, vol. 48, pp. 1098–1100, 1986.
[9] L. Olsson, S. Rudner, E. Kollberg, and C. O. Lindström, "A low noise SIS array receiver for radioastronomical applications in the 33-50 GHz band," *Int. J. Infrared Millimeter Waves*, vol. 4, pp. 847–858, 1983.
[10] S.-K. Pan, M. J. Feldman, A. R. Kerr, and P. Timbie, "Low-noise 115-GHz receiver using superconducting tunnel junctions," *Appl. Phys. Lett.*, vol. 43, pp. 786–788, 1983.
[11] R. Blundell, K. H. Gundlach, and E. J. Blum, "Practical low-noise quasi-particle receiver for 80–100 GHz," *Electron Lett.*, vol. 19, pp. 498–499, 1983.
[12] L. R. D'Addario, "An SIS mixer for 90-120 GHz with gain and wide bandwidth," *Int. J. Infrared Millimeter Waves*, vol. 5, pp. 1419–1442, 1984.
[13] J. W. Archer, "A high-performance, 2.5-K cryostat incorporating a 100-GHz dual polarization receiver," *Rev. Sci. Instrum.*, vol. 56, pp. 449–458, 1985.
[14] D. P. Woody, R. E. Miller, and M. J. Wengler, "85–115 GHz receivers for radio astronomy," *IEEE Trans. Microwave Theory. Tech.*, vol. MTT-33, pp. 90–95, 1985.
[15] E. C. Sutton, "A superconducting tunnel junction receiver for 230 GHz," *IEEE Trans. Microwave Theory Tech.*, vol. MTT-31, pp. 589 ff., 1983.
[16] H. A. Haus and R. B. Adler, "An extension of the noise figure definition," *Proc. IRE*, vol. 45, pp. 690–691, 1957.
[17] H. A. Haus and R. B. Adler, "Optimum noise performance of linear amplifiers," *Proc. IRE*, vol. 46, pp. 1517–1533, 1958.
[18] H. Rothe and W. Dahlke, "Theory of noisy fourpoles," *Proc. IRE*, vol. 44, pp. 811–818, 1956.
[19] J. Lange, "Noise characterization of linear twoports in terms of invariant parameters," *IEEE J. Solid State Circuits*, vol. SC-2, pp. 37–40, 1967.
[20] J. M. Rollett, "Stability and power-gain invariants of linear twoports," *IRE Trans. Circuit Theory*, vol. CT-9, pp. 29–32, 1962.
[21] N. R. Werthamer, "Nonlinear self-coupling of Josephson radiation in superconducting tunnel junctions," *Phys. Rev.*, vol. 147, pp. 255–263, 1966.
[22] A. A. M. Saleh, *Theory of Resistive Mixers*. Cambridge, MA: MIT Press, 1971.
[23] D. N. Held and A. R. Kerr, "Conversion loss and noise of microwave and millimeter-wave mixers," *IEEE Trans. Microwave Theory Tech.*, vol. MTT-26, pp. 49–61, 1978.
[24] R. G. Hicks, M. J. Feldman, and A. R. Kerr, "A general numerical analysis of the superconducting quasiparticle mixer," *IEEE Trans. Magn.*, vol. MAG-21, pp. 208–211, 1985.
[25] H. B. Callen and T. A. Welton, "Irreversibility and generalized noise," *Phys. Rev.*, vol. 83, pp. 34–40, 1951.
[26] J. Bardeen, L. N. Cooper, and J. R. Schrieffer, "Theory of superconductivity," *Phys. Rev.*, vol. 108, pp. 1175–1204, 1957.
[27] R. E. Harris, "Cosine and other terms in the Josephson tunneling current," *Phys. Rev. B*, vol. 10, pp. 84–94, 1974.
[28] R. H. Havemann, C. A. Hamilton, and R. E. Harris, "Photolithographic fabrication of lead alloy Josephson junctions," *J. Vac. Sci. Technol.*, vol. 15, pp. 392–395, 1978.
[29] A. D. Smith and P. L. Richards, "Analytical solutions to superconductor–insulator–superconductor quantum mixer theory," *J. Appl. Phys.*, vol. 53, pp. 3806–3812, 1982.
[30] M. W. Pospieszalski and S. Weinreb, "FETs and HEMTs at cryogenic temperatures—Their properties and use in low-noise amplifiers," in *Proc. Int. Microwave Symp.*, 1987, pp. 955–958.
[31] S. Weinreb, private communication, 1987.
[32] S. Weinreb, "SIS mixer to HEMT amplifier optimum coupling network," *IEEE Trans. Microwave Theory Tech.*, vol. MTT-35, pp. 1067–1069, 1987.
[33] H. Hillbrand and P. H. Russer, "An efficient method of computer aided noise analysis of linear amplifier networks," *IEEE Trans. Circuits Syst.*, vol. CAS-23, pp. 235–238, 1976.
[34] L. R. D'Addario, "Saturation of the SIS mixer by out-of-band signals,", *IEEE Trans. Microwave Theory Tech.*, vol. MTT-36, pp. 1103–1105, 1988.

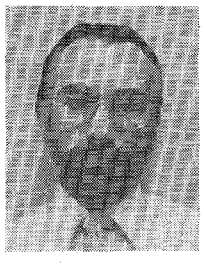

Larry R. D'Addario was born in New Jersey in 1946. He received the B.S. degree in electrical engineering from the Massachusetts Institute of Technology in 1968, and the S.M. and Ph.D. degrees from Stanford University in 1969 and 1974, respectively. His thesis work and later research at Stanford included major contributions to the development of a five-element synthesis radio telescope and its use in astronomical observations of Jupiter, galactic HII regions, and quasars.

Since 1974 he has been with the National Radio Astronomy Observatory in various capacities. From 1975 through 1979 he was systems engineer for electronics at the Very Large Array in New Mexico. Most recently, he has been with the NRAO's Central Development Laboratory in Charlottesville, VA, working on millimeter-wavelength devices including SIS mixers. During 1985 and 1986, he was also in charge of systems engineering for the Very Long Baseline Array. From June 1986 through July 1987, Dr. D'Addario was a visiting scientist at the CSIRO Division of Radiophysics, Epping, NSW, Australia, where he developed SIS junction fabrication facilities and conducted theoretical studies of SIS mixers.